



# Kent Academic Repository

Guevel, X.L., Wang, F.Y., Stranik, O., Nooney, R., Gubala, V., McDonagh, C. and MacCraith, B.D. (2009) *Synthesis, stabilization, and functionalization of silver nanoplates for biosensor applications*. *Journal of Physical Chemistry C*, 113 (37). pp. 16380-16386. ISSN 1932-7447.

## Downloaded from

<https://kar.kent.ac.uk/45243/> The University of Kent's Academic Repository KAR

## The version of record is available from

<https://doi.org/10.1021/jp904761p>

## This document version

Author's Accepted Manuscript

## DOI for this version

## Licence for this version

UNSPECIFIED

## Additional information

Unmapped bibliographic data:LA - English [Field not mapped to EPrints]J2 - J. Phys. Chem. C [Field not mapped to EPrints]AD - Biomedical Diagnostics Institute, School of Physical Sciences, Dublin City University, Glasnevin, Dublin 9, Ireland [Field not mapped to EPrints]DB - Scopus [Field not mapped to EPrints]

## Versions of research works

### Versions of Record

If this version is the version of record, it is the same as the published version available on the publisher's web site. Cite as the published version.

### Author Accepted Manuscripts

If this document is identified as the Author Accepted Manuscript it is the version after peer review but before type setting, copy editing or publisher branding. Cite as Surname, Initial. (Year) 'Title of article'. To be published in *Title of Journal*, Volume and issue numbers [peer-reviewed accepted version]. Available at: DOI or URL (Accessed: date).

## Enquiries

If you have questions about this document contact [ResearchSupport@kent.ac.uk](mailto:ResearchSupport@kent.ac.uk). Please include the URL of the record in KAR. If you believe that your, or a third party's rights have been compromised through this document please see our [Take Down policy](https://www.kent.ac.uk/guides/kar-the-kent-academic-repository#policies) (available from <https://www.kent.ac.uk/guides/kar-the-kent-academic-repository#policies>).

# Synthesis, Stabilization, and Functionalization of Silver Nanoplates for Biosensor Applications

Xavier Le Guével, Freddy Y. Wang, Ondrej Stranik, Robert Nooney, Vladimir Gubala, Colette McDonagh, and Brian D. MacCraith\*

Biomedical Diagnostics Institute, School of Physical Sciences, Dublin City University, Glasnevin, Dublin 9, Ireland

Received: May 21, 2009; Revised Manuscript Received: July 31, 2009

Silver nanoplates (NPTs) were prepared by a seed-mediated growth method with different diameters ( $d = 25, 32, 53,$  and  $100$  nm) and with thicknesses of approximately  $10$  nm in all cases. As the concentration of silver seeds increased, the diameter of the nanoplates increased, resulting in an overall shift in the localized surface plasmon resonance (LSPR) band maximum from  $570$  to  $900$  nm, thus providing a novel method to tune the plasmon resonance. The LSPR was calculated from theory for both triangular and circular nanoplate geometries. In agreement with transmission electron micrographs, the model results confirmed the shape of nanoplates as being truncated prisms, intermediate between that of a prism and a disk. Because of the toxicity of the surfactant hexadecyltrimethylammonium bromide (CTAB), the stabilizing CTAB bilayer surrounding the NPT was replaced by a nontoxic alkanethiol with surfactant properties. This enabled the extraction of metal nanoparticles into deionized water or buffer for bioconjugation without aggregation. Silver nanoplates were also coated with polyelectrolyte layers using the standard layer-by-layer (LbL) method. The LSPR was found to be very sensitive to the addition of polyelectrolyte layers, with a plasmon band shift from  $728$  to  $740$  nm after adding only one monolayer (thickness  $\sim 1.5$  nm). Bioconjugation of these nanoplates was achieved with the addition of a mercaptolinker containing a carboxyl group. The carboxyl groups were activated with 1-ethyl-3-(3-dimethylaminopropyl) hydrochloride (EDC)/*N*-hydroxysuccinimide (NHS) and conjugated to green fluorescent protein (GFP) in order to validate the potential of the NPTs for enhancement of bioassays. The fluorescence of the conjugated NPTs was 5.6-fold brighter than that of NPTs added to GFP without activation.

## Introduction

Noble metal nanoparticles are widely used in a range of applications, including electronics,<sup>1,2</sup> biosensing,<sup>3,4</sup> and surface-enhanced Raman spectroscopy.<sup>5</sup> In particular, the use of gold and silver nanostructures for biomedical diagnostics applications has been widely reported.<sup>6–11</sup> Gold (Au) and silver (Ag) nanoparticles (NPs) typically exhibit a localized surface plasmon resonance (LSPR) phenomenon, which is caused by the collective oscillations of free electrons interacting with the incident light.<sup>12,13</sup> The LSPR wavelength ( $\lambda_{\text{res}}$ ) of the NPs can be modulated by changing their size, shape, composition, interparticle distance, and dielectric constant.<sup>14,15</sup> Due to their LSPR, they are of most interest in biodiagnostics as tags for labeling biomolecules, as localized sensors,<sup>16</sup> or to enhance the fluorescence of other fluorescent labels.<sup>17</sup> With a view to increasing the sensitivity of fluorescence inside cells and tissue<sup>18–20</sup> there is also interest in shifting the LSPR to the near-infrared (NIR) region where there is less autofluorescence from biomaterials. We chose silver nanoparticles in preference to gold because silver has superior optical properties at visible wavelengths. Due to the importance of the NP shape, many efforts have been made to develop novel, shape-controlled approaches for metal NP synthesis.<sup>21,22</sup> In comparison to one-dimensional (1D) nanostructures (wires, rods, belts, or tubes), two-dimensional (2D) silver nanostructures such as triangles,<sup>23</sup> plates,<sup>24</sup> and discs<sup>25–27</sup> are not well-understood in terms of synthesis and growth mechanisms.

There are many routes for the synthesis of metal nanoplates including seed-mediated growth,<sup>23,28,29</sup> thermal growth,<sup>30</sup> and photoinduced methods.<sup>31,32</sup> In this work, we used the seed-mediated growth approach to make nanoplates (NPTs), following a modification of the procedure described by Jana et al.<sup>33</sup> We choose to concentrate on the NPT morphology because (I) they possess easily tunable optical properties which are compatible with widely used red fluorescent antibody labels, for example, Cy5, compared to  $\lambda_{\text{res}}$  of spherical nanoparticles and (II) there have been relatively few previous literature reports of these structures compared to nanorods. We found that the size of the NPTs is highly sensitive to changes in the concentration of reactants in the synthesis protocol.

In this paper, we focus on the synthesis and stabilization of silver nanoplates with different diameters. We initially used hexadecyltrimethylammonium bromide (CTAB) surfactant as a soft template to stabilize the nanoplates.<sup>34</sup> However, CTAB solutions are cytotoxic<sup>35</sup> and interfere with established protein-linking protocols. We have successfully replaced the CTAB with a mercaptolinker with surfactant properties with which we have coated the entire nanoplate surface. As far as we are aware, this is the first demonstration of the use of the complex for this purpose. We also report on a reproducible technique for coating the NPTs with polyelectrolyte (PEL) layers which significantly alter the dielectric field and hence give rise to a reproducible shift in  $\lambda_{\text{res}}$ . The extreme sensitivity to the local environment of the dipole plasmon band of the NPTs points to their potential use in refractometric biosensing applications. Furthermore, in

\* To whom correspondence should be addressed.

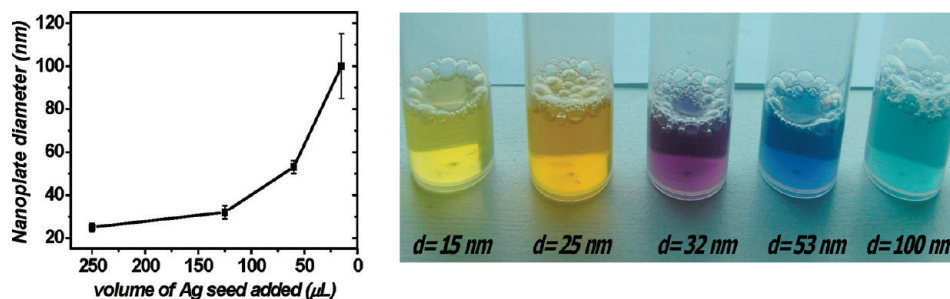


**Figure 1.** Variation of size of nanoplates as a function of the silver seed volume added.

order to demonstrate their potential for enhancement of fluorescence-based immunoassays, the NPTs were conjugated to green fluorescent protein (GFP) using an alkanethiol linker.

The novel aspects of this work lie in the tailoring of the synthesis procedure to produce silver NPTs of controllable size and the stabilization of the plates using a biocompatible surfactant mercaptolinker protective group which also minimizes particle aggregation. The absorption properties of the NPTs were modeled, and good agreement was obtained between the model and the experimental absorption data. The main motivation for the work lies in the potential enhancements obtainable by using metal nanostructures in optical bioassays as well as the potential to use the NPTs in refractometric biosensing.

## Experimental Section

**Materials.** All reactants (except the *N,N,N*-trimethyl(11-mercaptoundecyl)ammonium bromide obtained from Prochimia, Poland) were purchased from Sigma-Aldrich, Ireland and used as received. The polyelectrolytes, polyethyleneimine (PEI)  $M_w \sim 750\,000$ , poly(sodium-4-styrenesulfonate) (PSS)  $M_w \sim 70\,000$ , and poly(allylamine hydrochloride) (PAH)  $M_w \sim 70\,000$ , were also obtained from Sigma-Aldrich and used without further purification. Deionized water ( $18\text{ M}\Omega \cdot \text{cm}$ ) was used in all experiments. All glassware used in the synthesis of nanoplates was siliconized using dichlorodimethylsilane (2% w/w) in chloroform) and cured at  $80\text{ }^\circ\text{C}$  for 2 h.

**Synthesis of Silver Nanoparticle Seeds.** Spherical Ag nanoparticles, with an average particle size around 10 nm, were synthesized according to the seeding method described by Jin et al.<sup>31</sup> Briefly, 1 mL of 30 mM silver nitrate ( $\text{AgNO}_3$ ) was combined with 1 mL of 30 mM trisodium citrate (a weak reducing agent) in 48 mL of  $\text{H}_2\text{O}$ . In parallel, 50 mM sodium borohydride solution ( $\text{NaBH}_4$ ) (strong reducing agent) was prepared separately in ice-cold water. An amount of 1 mL of this  $\text{NaBH}_4$  solution was then quickly added, via a syringe, to the silver citrate solution in a round-bottomed flask under vigorous stirring. An amount of 1 mL of 5 mM bis(*p*-sulfonatophenyl)phenyl phosphine dipotassium dehydrate (BSPP) was then added to the colloid. The BSPP provides the protection groups avoiding aggregation. The colloid was then stirred for another 15 min. The yellow solution was used without any purification and between 1 and 5 h after the synthesis.

**Synthesis of Silver Nanoplates.** Four different nanoplate growth solutions were prepared by a seed-mediated route.<sup>33</sup> It is crucial to use fresh silver seeds, because the seeds grow quickly, thereby leading to a reduction of the amount of nanoplates in solution. For each sample, the following reagents were added to plastic tubes in the following order, with gentle mixing between each addition: 10 mL of 80 mM CTAB, 0.25 mL of 10 mM  $\text{AgNO}_3$ , and 0.5 mL of 100 mM ascorbic acid. In order to make nanoplates of varying diameter  $\varnothing$ , different

amounts of silver seeds were added: 30–60–125–250  $\mu\text{L}$ . For each sample, 0.1 mL of 1 mM NaOH was then added, which produced solution colors of green ( $d \sim 100 \pm 7\text{ nm}$ ), blue ( $d = 53 \pm 5\text{ nm}$ ), purple ( $d = 32 \pm 3\text{ nm}$ ), and orange ( $d = 25 \pm 2\text{ nm}$ ), as a function of the Ag seed concentration (Figure 1). This change corresponds to the formation of silver NPTs. After 2 h, the excess CTAB precipitated out and was separated from each solution.

**Stabilization of Silver Nanoplates.** The NPTs were kept at room temperature overnight. Then 200  $\mu\text{L}$  of *N,N,N*-trimethyl(11-mercaptoundecyl) ammonium bromide (20 mg/mL) was added to 6 mL of Ag NPTs, and the solution stirred for 2 h. Following this, the solution was centrifuged three times at 9000 rpm for 15 min in Eppendorf tubes and resuspended in water. The new functionalized NPTs are referred to as Ag NPTs–MMPC (mixed monolayer protected cluster).<sup>36,37</sup> As a control, Ag NPTs samples without mercaptolinker were purified using the same protocol.

**Polyelectrolyte-Coated Silver Nanoplates.** Stock solutions of PEI, PSS, and PAH, at 2 mg/mL concentration, were prepared in 6 mM aqueous NaCl solution. Ag NPTs–MMPC were positively charged due to the presence of ammonium groups on the surface. The positively charged surface was converted to a negatively charged surface with the addition of PSS solution. Briefly, 3 mL of PSS solution was added to 3 mL of Ag NPTs–MMPC in plastic tubes and stirred for a minimum of 2 h. The excess was removed by centrifuging, rinsing twice (9000 rpm, 10 min), and finally redispersing in 3 mL of water. The absence of any color changes overtime and the relatively constant absorbance spectra showed that the coated NPTs were stable over several weeks.

Using a standard polyelectrolyte (PE) layering technique,<sup>38–40</sup> microplates were plasma-treated and coated with PEI/PSS/PAH layers. This procedure allowed us to get a homogeneous positive charge on the surface. Following this, 200  $\mu\text{L}$  of Ag NPTs–MMPC labeled by PPS were added to the microplate, covered with Parafilm, and left overnight at room temperature.

**Biofunctionalization.** The protocol used for conjugation of GFP to the NPTs was as follows: To 6 mL of Ag NPTs–MMPC solutions, the alkanethiol 16-mercaptohexadecanoic acid (MHA) was added in excess (100  $\mu\text{L}$ , 1 mM in ethanol) and stirred for 10 min. Then, the new solutions were centrifuged twice and redispersed in water. After activation of the carboxy groups on the MHA for 30 min with the carboimide 1-ethyl-3-(3-dimethylaminopropyl) hydrochloride (EDC) and *N*-hydroxysuccinimide (NHS) (EDC/NHS = 4:1) in MES buffer (pH = 4.5), GFP was conjugated to the nanoplates (45  $\mu\text{L}$ ; 3 mg/mL). The functionalized silver nanoplates were purified three times using a zeba column (Thermo Scientific, U.S.A.).

Figure 2 shows a schematic of the synthesis, protection, and functionalization of the NPTs.

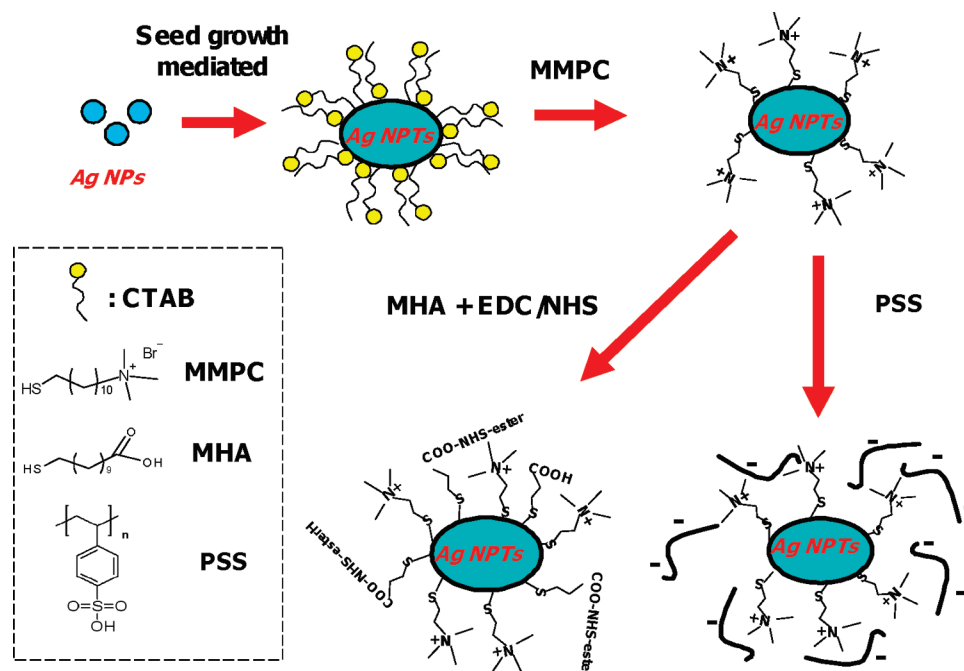


**Figure 2.** Synthesis of silver nanoplates (NPTs) using the seed-mediated growth method. NPTs are stabilized with the mercaptolinker MMPC. For functionalization, NPTs were coated with (I) a polyelectrolyte PSS (poly(sodium-4-styrenesulfonate)) and (II) a mercaptolinker MHA activated with EDC/NHS.

**Instrumentation.** The shift of the plasmon bands of the NPTs was monitored using UV-vis spectroscopy on a Varian model Cary 50 Scan spectrophotometer. Fluorescence of GFP was measured ( $\lambda_{exc} = 425$  nm;  $\lambda_{em} = 508$  nm) on a Tecan infinite M200 instrument using microplates. Transmission electron microscopy (TEM) was carried out with a FEI Tecnai Philips microscope operating at an accelerating voltage of 300 kV. The variation of surface charge on the silver nanoplates before and after functionalization was measured on a Zetasizer instrument from Malvern.

## Results and Discussion

**Synthesis, Characterization, and Theoretical Modeling of Silver Nanoplates.** A seed-mediated route was used to synthesize four silver nanoplate solutions ( $d = 25, 32, 53,$  and  $100$  nm with a thickness of  $10$  nm for all). The size of the metal nanoplates depends on the concentration of reagents, surfactant, synthesis temperature, and time.<sup>25–27,41</sup> In this work, the definition “nanoplate” covers geometrical structures ranging from discs to triangular prisms but does not include spherical or rod-type structures. TEM pictures of individual nanoplates are shown on Figure 3a–d. A high yield of NPTs (over 80%) was obtained for all solutions. The thickness was determined using TEM by measuring nanoplates stacked together. The size of the NPTs increased as the concentration of seeds decreased. The smaller NPTs were reasonably monodispersed, whereas the largest particles showed some polydispersity. This is indicated by the relatively large error bar for the large particles in Figure 1.

Figure 4 shows the absorption spectra of the NPTs in water as a function of increasing diameter. The spectra exhibit two main peaks; the first at around  $400$  nm is almost independent of plate diameter, and the second is tunable in the range from  $500$ – $1000$  nm as the diameter increases. The absorption spectra of the NPTs were also modeled, and the model was compared with the experimental data. Calculations were carried out using the freely available software package DDSCAT (discrete dipole approximation for scattering and absorption of light by irregular

particles),<sup>42</sup> which is based on the discrete dipole approximation method.<sup>43</sup> The spectra were calculated for two different geometries, nanodisc and equilateral triangular prism, with four diameters ( $25, 32, 53,$  and  $100$  nm, respectively) and a thickness of  $10$  nm. The nanoplates were assumed to be silver and immersed in water. The refractive index value of silver was obtained from Palik.<sup>44</sup> The computed position of the main LSPR peak and the full width at half-maximum (fwhm) for each geometry and size are plotted in Figure 5 together with the experimental data. The positions of both the calculated and measured LSPR shift to longer wavelength with increasing size of the NPs. The experimental peaks lie between the calculated position of LSPR for nanodiscs (shorter  $\lambda_{res}$ ) and nanotriangles (longer  $\lambda_{res}$ ) as seen in the inset in Figure 5. From our calculations (not presented) and also from the literature<sup>45</sup> it follows that the plasmon peak shifts from longer to shorter wavelength by progressively altering the shape of the NP from a triangular shape to a pseudocircular shape (equivalent to “snipping” the tips of the triangles). Furthermore, the fwhm of the calculated spectra are narrower than the experimental ones due to a degree of polydispersity and the calculated positions of LSPR for nanodiscs and nanotriangles are within the fwhm of the measured spectra. From an analysis of the theoretical and experimental data, we propose that our NPTs have shapes ranging from ideal circular discs to triangular discs. By comparing the theoretical and experimental absorption data, we predict that a large proportion of the NPTs are truncated triangular prisms. This broad distribution of shapes is consistent both with the large fwhm in Figure 5 and with the TEM images shown in Figure 3.

The size and concentration of the silver seed has a strong impact on nanoplate quality. Figure 6 shows the absorption spectra obtained for NPTs of diameter  $32$  nm under conditions of high (black line) and low (red line) seed concentration. For a high concentration of Ag seeds, the high-wavelength plasmon band grows at the expense of the  $410$  nm band. The opposite occurs for low seed concentration where most of the seeds do

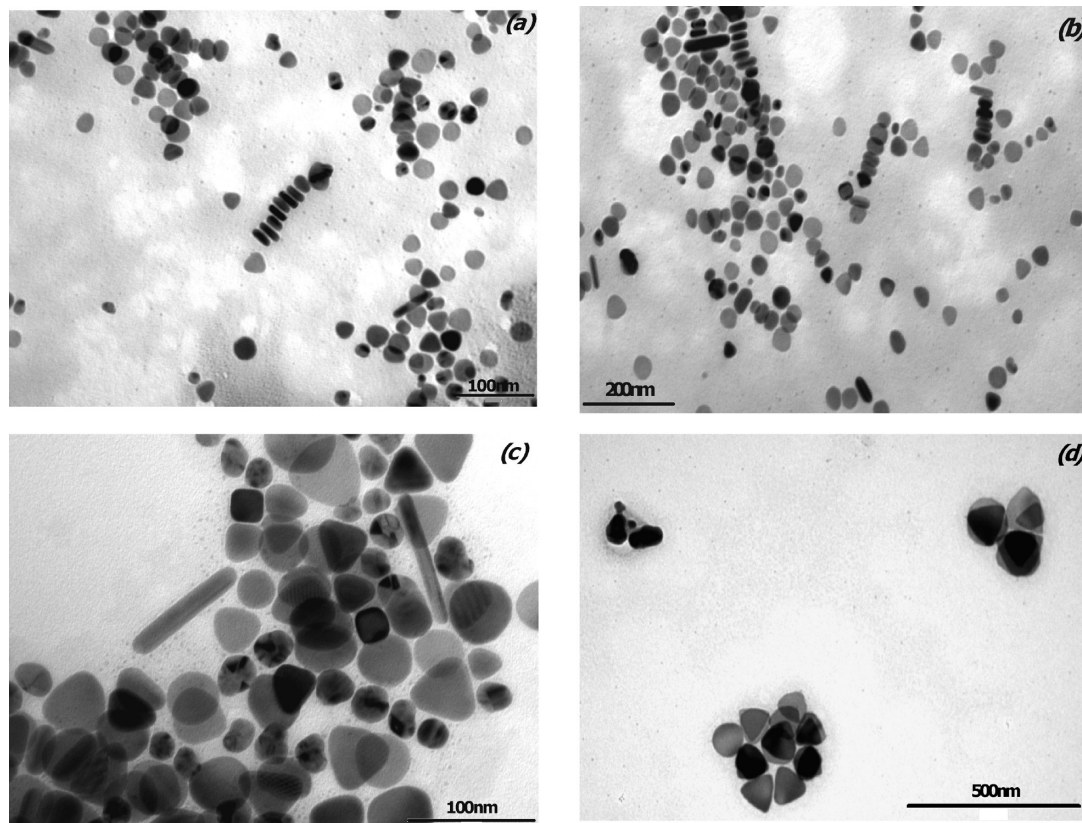


Figure 3. TEM pictures of Ag NPTs: (a)  $d = 25$  nm, (b)  $d = 32$  nm, (c)  $d = 53$  nm, and (d)  $d = 100$  nm.

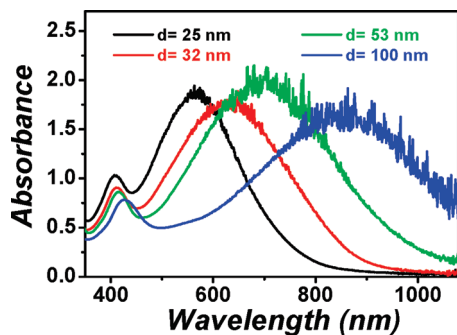


Figure 4. Visible NIR absorption spectra of the silver NPTs, of thickness 10 nm and with diameter  $d = 25, 32, 53, 100$  nm.

not form NPTs but remain in solution after synthesis. The presence of a large concentration of unreacted seeds gives rise to a large increase in the 410 nm band relative the high-wavelength NPT plasmon band.

**Protection of the Silver Nanoplates.** It is well-established that silver nanostructures are highly unstable and prone to aggregation and oxidation. The conventional method of stabilization is the use of a surfactant, typically CTAB. Several studies have investigated the effects of surfactant concentration on nanoparticle growth and influence of the surfactant on the nanoparticle during that growth process.<sup>34</sup> Nikoobakht and El-Sayed<sup>46</sup> established that, in the case of nanorods, the surfactant is associated with the formation of bilayers which is consistent with the cationic portion dominating the nanorods. The CTAB stabilizes the nanoparticles but, on removal, leads to nanoparticle aggregation in all cases. As the NPTs synthesized in this work are targeted at biosensing applications, the toxicity of CTAB may pose a problem. It was decided to exchange CTAB with a mercaptolinker MMPC which has surfactant properties and which covalently binds to the silver. This linker has the same

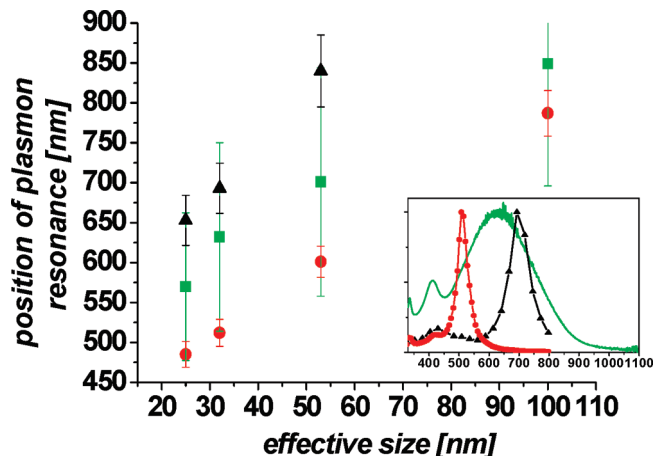
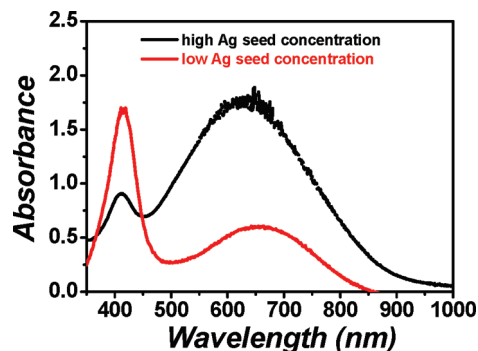


Figure 5. Graph of experimentally measured and theoretically calculated positions of the plasmon resonance as a function of NP size. The data points indicate maximum absorption, where squares represent experimental values, circles represent calculated values for nanoplates, and triangles represent triangular nanoprisms. The inset represents the calculated and measured absorption spectra for NP of diameter 32 nm.

chemical properties as CTAB, e.g., an alkyl chain and an ammonium group, and therefore replaces all CTAB molecules. Figure 7a presents the absorption spectra of Ag NPTs ( $d = 32 \pm 2$  nm) with and without MMPC. We can clearly see a shift of the dipole plasmon band to the higher wavelength from 625 to 690 nm after functionalization. This behavior corresponds to a change in the refractive index sensed by the nanoparticle which is the result of the change in surface coating from CTAB to MMPC. The stabilization of Ag NPTs was established by carrying out two experiments: centrifugation, which led to a decrease of the CTAB concentration in solution, and second,



**Figure 6.** Absorption spectra of Ag NPTs for  $d = 32$  nm with high seed concentration (black line) and low seed concentration (red line).

the addition of concentrated potassium cyanide solution which is well-known to etch silver. For the protected Ag NPTs–MMPC, the plasmon band in the near-infrared region, which relates to the presence of NPTs, remains the same both after three centrifugations (Figure 7, parts a and b) and also in the presence of KCN (2.5 mM) (Figure 8, parts a and b). The stability without CTAB can be related to the high  $\zeta$ -potential (Figure 9a) of Ag NPTs and Ag NPTs–MMPC at around +40 mV. This means that the NPTs are strongly positively charged and are able to

repel each other through solvation and electrostatic repulsion. Without the presence of the mercaptolinker, the plasmon band at 700 nm due to Ag NPTs decreases and disappears after centrifugation. The NPTs are protected from the cyanide molecules because the alkyl chains pack closely together forming a steric and hydrophobic barrier which prevent the cyanide from reacting with the silver atoms

**Polyelectrolyte Coating of Silver Nanoplates.** As discussed above, the spectral position of the NPT plasmon band is highly sensitive to the refractive index of the local environment. This effect can be used as a refractometric biosensor whereby binding to receptors (for example, antibodies) on the NPTs can be detected by a shift in the  $\lambda_{\text{res}}$ . This detection principle has been investigated by coating the NPTs with polyelectrolytes using a versatile layer-by-layer approach. The anionic polyelectrolyte PSS is electrostatically adsorbed onto the protected Ag NPTs–MMPC via electrostatic interactions.<sup>36,37</sup> The stabilization of the nanoplates with the mercaptolinker is necessary before coating with the polyelectrolyte. The presence of the polyelectrolyte layer was confirmed through Dynamic Light Scattering (DLS) measurements. Thus, in Figure 9a, we note a stability of the  $\zeta$ -potential of Ag NPTs at around +40 mV before and after adding the mercaptolinker. The surface is positively charged due to the presence of an ammonium group. It can be clearly observed that there is a charge reversal upon deposition of the

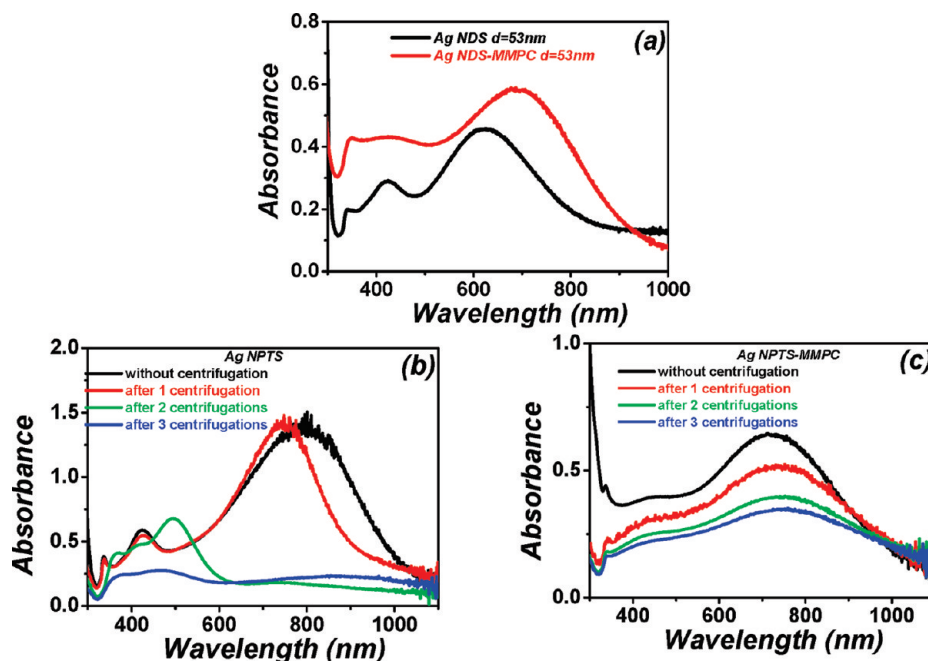


**Figure 7.** Absorption spectra of Ag NPTs with and without (a) MMPC for  $d = 32$  nm and after repeated centrifugation steps (b and c).

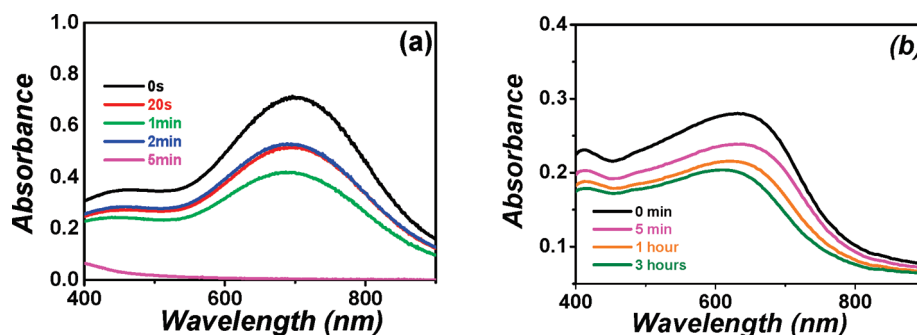


**Figure 8.** Visible NIR absorption spectra of Ag NPTs for  $d = 32$  nm, before (a) and after (b) addition of the mercaptolinker MMPC in the presence of potassium cyanide KCN (2.5 mM).

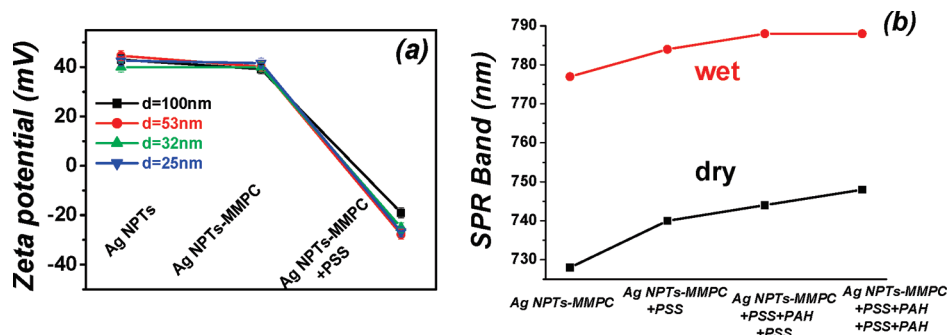


**Figure 9.** Change in  $\zeta$ -potential of silver nanoplates with the addition of MMPC followed by the addition of an anionic polyelectrolyte (PSS) monolayer (a). Shift of the maximum of the dipole plasmon peak for Ag NPTs–MMPC  $d = 32$  nm with different numbers of polyelectrolyte layers in dry and wet conditions (b).

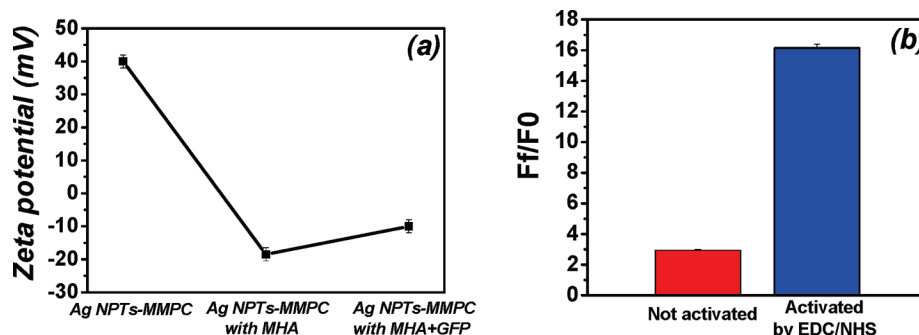


**Figure 10.** Change in  $\zeta$ -potential for silver nanoplates ( $d = 53$  nm) after functionalization with MHA and GFP (a). Fluorescence intensity of Ag NPTs–MMPC conjugated with MHA and GFP with and without EDC/NHS activation (b).

oppositely charged polyelectrolyte onto the surface of Ag NPTs–MMPC. In fact, the  $\zeta$ -potential drops down from +40 to  $-25$  mV after the PSS deposition. As expected, this behavior is independent of the diameter with the same values of the  $\zeta$ -potential for the samples after each step.

A layer-by-layer technique has also been used to coat NPTs with an overlayer of the positive polyelectrolyte, PAH. Controlling several parameters, such as the pH of the solution, salt concentration in the solution, and the type of polyelectrolyte, we can choose the thickness of the layer (1.5 nm in our case) as established previously in our laboratory.<sup>40</sup> Multiple PE layers were deposited as above. Absorption measurements have been performed after addition of each layer both in dry and wet conditions. The UV–vis spectra as a function of the different polymer coatings are shown in Figure 9b. It is well-known that, as the local dielectric constant increases, it results in a red-shift of the NP plasmon band. The change is due to variation of the local refractive index from that of water ( $n \sim 1.33$ ) to that of polyelectrolyte ( $n \sim 1.5$ ) upon polymer adsorption. Furthermore, the peak wavelength shift is highly sensitive to the amount of material adsorbed to the particle surface. We show only the results for Ag NPTs–MMPC (Figure 9b) covered with PSS, but the behavior is exactly the same for all samples. Moreover, the width of the absorption peak remains the same, and only the shift at the maximum intensity is plotted. Under dry conditions, the plasmon band shifts from 728 to 740 nm after adding only one monolayer which is approximately 1.5 nm thick. There was a shift of about 4 nm for each subsequent layer. Under wet conditions, the resonance peak moved to 777 nm because of the change of the refractive index from air ( $n = 1$ ) to water ( $n = 1.33$ ). After adding PE layers, the band shifted to 788 nm after three PE layers. These results indicate the high sensitivity of the plasmon band of the NPTs to the local change of the refractive index. In this work, adsorption of a single layer of thickness 1.5 nm can be detected. Clearly, there is potential

to use this sensitive shift in plasmon absorption wavelength to detect binding events in a bioassay format.

**Grafting Proteins to the Silver Nanoplates.** As indicated in the Introduction, the main targeted application for future work is to use the NPTs for enhancement of optical bioassays, in particular fluorescence-based immunoassays, using the principle of plasmonic enhancement of fluorescence.<sup>40,47</sup> Hence, a protein conjugation protocol was developed and tested using GFP. The process consisted of two steps; first, MHA was attached to the NPT surface providing reactive carboxylic groups, and second, the biomolecule GFP, was covalently attached to the MHA. The layer-by-layer functionalization discussed in the previous section indicated that it was not possible to graft MHA directly on the Ag NPTs without destroying the main part of the NPTs. This behavior can be attributed to the tightly packed CTAB bilayer on the surface of the silver nanoplates which hinders access to the alkanethiol molecule. Furthermore, there is electrostatic attraction between carboxyl group on MHA and the positively charged ammonium on CTAB, which is added in huge excess. Therefore, MHA was added to Ag NPTs–MMPC and reacted to make a covalent bond with the surface. However, we observed that it was crucial to work with a low concentration of MHA, for a short period of time, to prevent a precipitation of the colloids. Working in water at pH 6.5, the terminal carboxylic groups of MHA oriented on the outside of the NPTs are negatively charged and the  $\zeta$ -potential drops from +40 to  $-18.5$  mV (Figure 10a). This significant drop in  $\zeta$ -potential value indicates that the MHA has coated a large proportion of the nanoplate surface. The carboxylic groups have to be activated with EDC/NHS before introducing GFP in the solution. This is a well-known technique to conjugate carboxyl to amine groups in peptides and proteins. Indeed, at lower pH, EDC reacts with a carboxylic acid to form an amine-reactive intermediate. Then, in the presence of NHS, the amine-reactive intermediate can be converted to amine-reactive NHS esters. Previous work in

our laboratory has involved optimizing the activation process by tailoring the pH of the solution, the reaction time needed for the COOH activation, the molar excess of NHS per COOH group, and the ratio of the EDC/NHS coreactants. After the addition of GFP, there was a decrease in the number of deprotonated carboxylic groups on the nanoplates which was evidenced by a slight drop of the values of the  $\zeta$ -potential from  $-18.5$  to  $-10$  mV. Figure 10b displays the fluorescence data of Ag NPTs–MMPC ( $d = 53$  nm) conjugated to GFP with and without activation (EDC/NHS). With activation, the fluorescence is 5.6-fold brighter than without activation. Moreover, the control sample shows a low fluorescence intensity indicating a weak nonspecific binding of GFP on the surface of the silver nanoplates.

## Conclusion

Silver nanoplates with different diameters were synthesized with a high yield, stabilized, and then functionalized for bioconjugation to a protein using an alkanethiol. The stabilization via a mercaptolinker, Ag NPTs–MMPC, allows the removal of the surfactant and prevents etching of the silver. The bioconjugation of silver nanoplates with the model protein GFP indicates that the protein covers the entire surface with low nonspecific binding. It was also demonstrated that the NPTs can be coated reproducibly with thin PEL layers which give rise to a red-shift in the plasmon peak. This extreme sensitivity of the plasmon peak to the refractive index of the surrounding medium could be used for biosensor applications. In particular, as the plasmon band of the NPTs matches well to the spectral properties of Cy5 and Cy5-like fluorescent labels, there is significant potential for the use of these nanostructures in highly sensitive metal-enhanced fluorescence-based immunoassays.

**Acknowledgment.** This material is based upon works supported by the Science Foundation Ireland under Grant No. 05/CE3/B754.

## References and Notes

- (1) Chung, S. W.; Yu, Y.; Heath, J. R. *Appl. Phys. Lett.* **2006**, *76*, 2068.
- (2) Yao, J. L.; Pan, G. P.; Xue, K. H.; Wu, D. Y.; Ren, B.; Sun, D. M.; Tang, J.; Xu, X.; Tian, Z. Q. *Pure Appl. Chem.* **2000**, *72*, 221–228.
- (3) Stuart, D. A.; Haes, A. J.; Yonzon, C. R.; Hicks, E. M.; Van Duyne, R. P. *IEE Proc.: Nanobiotechnol.* **2005**, *152*, 13–32.
- (4) Elghanian, R.; Storhoff, J. J.; Mucic, R. C.; Letsinger, R. L.; Mirkin, C. A. *Science* **1997**, *277*, 1078–1081.
- (5) Schwartzberg, A. M.; Zhang, J. Z. *J. Phys. Chem. B* **2008**, *112*, 10323–10337.
- (6) Wang, Z. L. *J. Phys. Chem. B* **2000**, *104*, 1153–1175.
- (7) Huang, X. H.; El-Sayed, I. H.; Qian, W.; El-Sayed, M. A. *J. Am. Chem. Soc.* **2006**, *128*, 2115–2120.
- (8) Durr, N. J.; Larson, T.; Smith, D. K.; Korgel, B. A.; Sokolov, K.; Ben-Yakar, A. *Nano Lett.* **2007**, *7*, 941–945.
- (9) Hirsch, L. R.; Stafford, R. J.; Bankson, J. A.; Sershen, S. R.; Rivera, B.; Hazle, J. D.; Halas, N. J.; West, J. L. *Proc. Natl. Acad. Sci. U.S.A.* **2003**, *100*, 13549.

- (10) Pearce, M. E.; Melanko, J. B.; Salem, A. K. *Pharm. Res.* **2007**, *24*, 2335–2352.
- (11) Yu, C.; Irudayaraj, J. *Biophys. J.* **2007**, *93*, 3684–3692.
- (12) Kreibig, U.; Vollmer, M. *Optical Properties of Metal Clusters*; Springer-Verlag: Berlin, Heidelberg, 1995.
- (13) Hutter, E.; Fendler, J. H. *Adv. Mater.* **2004**, *16*, 1685–1706.
- (14) Kelly, K. L.; Coronado, E.; Zhao, L. L.; Schatz, G. C. *J. Phys. Chem. B* **2003**, *107*, 668–677.
- (15) Noguez, C. *Opt. Mater.* **2005**, *7*, 1204–1211.
- (16) Nath, N.; Chilkoti, A. *J. Fluoresc.* **2004**, *14*, 377–389.
- (17) Penn, S. G.; He, L.; Natan, M. J. *Curr. Opin. Chem. Biol.* **2003**, *7*, 609–615.
- (18) Weissleder, R. *Nat. Biotechnol.* **2001**, *19*, 316–317.
- (19) Huang, Y.-F.; Chang, H.-T.; Tan, W. *Anal. Chem.* **2008**, *80*, 567–572.
- (20) Huang, X.; El-Sayed, I. H.; Qian, W.; El-Sayed, M. A. *Nano Lett.* **2007**, *7*, 1591–1597.
- (21) Sau, T. K.; Murphy, C. J. *J. Am. Chem. Soc.* **2004**, *126*, 8648–8649.
- (22) Sun, Y.; Mayers, B.; Xia, Y. *Nano Lett.* **2003**, *3*, 675–679.
- (23) Jin, R.; Cao, Y.; Mirkin, C. A.; Kelly, K. L.; Schatz, G. C.; Zheng, J. G. *Science* **2001**, *294*, 1901–1903.
- (24) Yener, D. O.; Sindel, J.; Randall, C. A.; Adair, J. H. *Langmuir* **2002**, *18*, 8692–8699.
- (25) Maillard, M.; Giorgio, S.; Pileni, M. P. *Adv. Mater.* **2002**, *14*, 1084–1086.
- (26) Pastoriza-Santos, I.; Liz-Marzan, L. M. *Nano Lett.* **2002**, *2*, 903.
- (27) Maillard, M.; Giorgio, S.; Pileni, M. P. *J. Phys. Chem. B* **2003**, *107*, 2466.
- (28) Chen, S.; Carroll, L. *Nano Lett.* **2002**, *2*, 1003–1007.
- (29) Zeng, Q.; Jiang, X.; Yu, A.; Lu, G. *Nanotechnology* **2007**, *18*, 1–7.
- (30) Hao, E.; Kelly, K. L.; Hupp, J. T.; Schatz, G. C. *J. Am. Chem. Soc.* **2002**, *124*, 15182–15183.
- (31) Jin, R.; Cao, Y.; Mirkin, C. A.; Hao, E.; Metraux, G. S.; Schatz, G. C.; Mirkin, C. A. *Nature* **2003**, *425*, 487–490.
- (32) Callegari, A.; Tonti, D.; Cherqui, M. *Nano Lett.* **2003**, *3*, 1565–1568.
- (33) Jana, N. R.; Gearheart, L.; Murphy, C. J. *Chem. Commun.* **2001**, 617–618.
- (34) Murphy, C. J.; Gole, A. M.; Hunyadi, S. E.; Orendorff, C. J. *Inorg. Chem.* **2006**, *45*, 7544–7554.
- (35) Mirska, D.; Schirmer, K.; Funari, S. S.; Langner, A.; Dobner, B.; Brezesinski, G. *Colloids Surf., B* **2005**, *40*, 51–59.
- (36) McIntosh, C. M.; Esposito, E. A.; Boal, A. K.; Simard, J. M.; Martin, C. T.; Rotello, V. M. *J. Am. Chem. Soc.* **2001**, *123*, 7626–7629.
- (37) Sandhu, K. K.; McIntosh, C. M.; Simard, J. M.; Smith, S. W.; Rotello, V. M. *Bioconjugate Chem.* **2002**, *13*, 3–6.
- (38) Shchukin, D. G.; Sukhorukov, G. *Adv. Mater.* **2004**, *16*, 671–682.
- (39) Bertrand, P.; Jonas, A.; Laschewski, A.; Legras, R. *Macromol. Rapid Commun.* **2000**, *21*, 319–348.
- (40) Nooney, R. I.; Stranik, O.; McDonagh, C.; McCraith, B. D. *Langmuir* **2008**, *24*, 11261–11267.
- (41) Lee, G. J.; Shin, S. I.; Kim, Y. C.; Oh, S. G. *Mater. Chem. Phys.* **2004**, *84*, 197–204.
- (42) Draine, B. T.; Flatau, P. T. *Program DDSCAT*; Scripps Institute of Oceanography, University of California: San Diego, CA, 2004.
- (43) Purcell, E. M.; Pennypacker, C. R. *Astrophys. J.* **1973**, *186*, 705–714.
- (44) Palik, E. D. *Handbook of Optical Constants of Solids*; Academic Press, Inc.: New York, 1985.
- (45) Kelly, K. L.; Coronado, E. *J. Phys. Chem. B* **2003**, *107*, 668–677.
- (46) Nikoobakht, B.; El-Sayed, M. A. *Chem. Mater.* **2003**, *15*, 1957–1962.
- (47) Stranik, O.; Nooney, R.; McDonagh, C.; MacCraith, B. D. *Plasmonics* **2007**, *2*, 15–22.

JP904761P